

# We are IntechOpen, the world's leading publisher of Open Access books Built by scientists, for scientists

6,900

Open access books available

186,000

International authors and editors

200M

Downloads

Our authors are among the

154

Countries delivered to

TOP 1%

most cited scientists

12.2%

Contributors from top 500 universities



WEB OF SCIENCE™

Selection of our books indexed in the Book Citation Index  
in Web of Science™ Core Collection (BKCI)

Interested in publishing with us?  
Contact [book.department@intechopen.com](mailto:book.department@intechopen.com)

Numbers displayed above are based on latest data collected.  
For more information visit [www.intechopen.com](http://www.intechopen.com)



## Orbital Magnetism of Graphenes

Mikito Koshino

*Department of Physics, Tohoku University*

*Sendai, 980-8578*

*Japan*

### 1. Introduction

The magnetism of conventional metal is composed of two different contributions, the Pauli paramagnetism due to the spin magnetic moment, and the Landau diamagnetism due to the orbital motion of electrons. In a free electron system, the magnitude of the spin component is larger than the orbital component so that the system exhibits paramagnetism in total. In a condensed matter system, on the other hand, the orbital magnetism sensitively depends on the detail of the band structure, and sometimes largely deviates from the conventional Landau diamagnetism. Particularly, narrow gap materials such as graphite(1–3) or bismuth (4–6) possess a strong orbital diamagnetism which overcomes the spin paramagnetism. Graphene monolayer (7–9) is an extreme case, in which the conduction and valance bands stick together with zero gap and a linear dispersion analogous to massless Dirac fermions. (1; 10–13) Accordingly, the orbital susceptibility has a strong singularity at band touching point (Dirac point), which has a Fermi energy dependence at zero temperature as (1; 14–25)

$$\chi(\varepsilon_F) \propto \delta(\varepsilon_F). \quad (1)$$

This anomalous behavior can be understood as a zero-mass limit of conventional magnetism for massive Dirac electron, in which the pseudo-spin magnetic moment associated valleys ( $K$  and  $K'$ ) gives an essential contribution (25). Monolayer graphene exhibits a non-trivial response also to non-uniform magnetic fields. Owing its scale-less electronic structure, graphene works as a magnetic mirror, where the response current creates a mirror magnetic field which mimics any external field distributions. (24)

The orbital magnetism was also studied for graphene-based materials, such as graphite intercalation compounds,(14–17) and multilayer graphenes. (26–28) Those systems have strong diamagnetism as well, while the delta-function singularity is strongly modified by the electronic coupling between different graphene layers. Bilayer graphene (29–32) has a zero-gap structure with a finite mass in contrast to massless band in monolayer (33–41). This leads to a less singular, logarithmic peak of the susceptibility.(15; 21) In graphene stacks with more than three layers, the Hamiltonian and thus susceptibility can be decomposed into contributions from sub-systems equivalent to monolayer or bilayer graphene.(21)

In this chapter, we review those anomalous properties of the orbital magnetism in graphene and related materials. In Sec. 2, we discuss the susceptibility of the monolayer graphene. We describe the origin of the delta function singularity at the Dirac point, and also a peculiar response to non-uniform magnetic field. We argue the orbital magnetism of bilayer graphene

in Sec. 3, and of general graphene stacks in Sec. 4. In Sec. 5, we extend the analysis to a three-dimensional Dirac system, which is known to give an effective model for bismuth.

## 2. Monolayer graphene

### 2.1 Magnetic susceptibility of graphene

Electronic states of graphene in the vicinity of  $K$  and  $K'$  points in the Brillouin zone are well described by the effective mass approximation. (1; 10–13) Let  $|A\rangle$  and  $|B\rangle$  be the Bloch functions at the  $K$  point, corresponding to  $A$  and  $B$  sublattices, respectively. In a basis  $(|A\rangle, |B\rangle)$ , the Hamiltonian for the monolayer graphene around the  $K$  point becomes

$$\mathcal{H}^K = \begin{pmatrix} \Delta & v\pi_- \\ v\pi_+ & -\Delta \end{pmatrix}, \quad (2)$$

where  $v \approx 1 \times 10^6$  m/s is the band velocity (8; 9),  $\pi_{\pm} = \pi_x \pm i\pi_y$ , and  $\pi = -i\hbar\nabla + (e/c)\mathbf{A}$  with vector potential  $\mathbf{A}$  giving external magnetic field  $\mathbf{B} = \nabla \times \mathbf{A}$ . In the following, we neglect the spin Zeeman energy because the spin splitting is much smaller than Landau-level separations. The Hamiltonian at the  $K'$  point is obtained by exchanging  $\pi_{\pm}$  in Eq. (2).

The diagonal terms  $\pm\Delta$  represent the potential asymmetry between  $A$  and  $B$  sites, which opens an energy gap at the Dirac point. Although  $A$  and  $B$  are intrinsically symmetric in usual graphene, the asymmetry can arise in a sample placed on a certain substrate material, where the interaction between the graphene and the substrate lattice produces different potentials between  $A$  and  $B$ . (42; 43) Theoretically, the singular behavior in ideal graphene with vanishing gap is intuitively understood by taking the limit  $\Delta \rightarrow 0$ , as will be shown below. We can safely assume  $\Delta \geq 0$  without loss of generality. The energy band at  $B = 0$  is given by

$$\varepsilon_s(p) = s\sqrt{v^2p^2 + \Delta^2}, \quad (s = \pm 1) \quad (3)$$

with electron momentum  $\mathbf{p} = (p_x, p_y)$  and  $p = \sqrt{p_x^2 + p_y^2}$ . The density of states is

$$D(\varepsilon) = \frac{g_v g_s |\varepsilon|}{2\pi\hbar^2 v^2} \theta(|\varepsilon| - \Delta), \quad (4)$$

where  $g_s = 2$  and  $g_v = 2$  represent the degrees of freedom associated with spin and valley, respectively, and  $\theta(t)$  is a step function, defined by

$$\theta(t) = \begin{cases} 1 & (t > 0); \\ 0 & (t < 0). \end{cases} \quad (5)$$

The Landau-level spectrum can be found using the relation  $\pi_+ = (\sqrt{2}\hbar/l_B)a^\dagger$  and  $\pi_- = (\sqrt{2}\hbar/l_B)a$ , where  $l_B = \sqrt{c\hbar/(eB)}$  is magnetic length and  $a^\dagger$  and  $a$  are raising and lowering operators for usual Landau-level wave functions, respectively. The eigenfunction of the Hamiltonian at  $K$  point is written as  $(c_1\phi_{n-1}, c_2\phi_n)$  with integers  $n \geq 0$ , where  $\phi_n$  is the usual Landau-level wave function and  $\phi_n$  of  $n < 0$  is regarded as 0. The Hamiltonian matrix for  $(c_1, c_2)$  becomes

$$H^K = \begin{pmatrix} \Delta & \hbar\omega_B\sqrt{n} \\ \hbar\omega_B\sqrt{n} & -\Delta \end{pmatrix}. \quad (6)$$

For  $n = 0$ , the eigenvector  $(c_1, c_2) = (1, 0)$ , corresponding to the eigenvalue  $\Delta$ , is not associated with any real eigenstates since the first component of wavefunction  $\phi_{-1}$  is zero. Similarly, the eigenfunction of  $K'$  point is written as  $(c_1\phi_n, c_2\phi_{n-1})$ , and the eigenvector  $(0, 1)$  of  $n = 0$ , corresponding to the eigenvalue  $-\Delta$ , is not a real state. From these arguments, we obtain the eigen energies,

$$\begin{aligned}\epsilon_n^K &= \text{sgn}_-(n)\sqrt{(\hbar\omega_B)^2|n| + \Delta^2}, \\ \epsilon_n^{K'} &= \text{sgn}_+(n)\sqrt{(\hbar\omega_B)^2|n| + \Delta^2}\end{aligned}\tag{7}$$

with  $n = 0, \pm 1, \pm 2, \dots$ ,  $\hbar\omega_B = \sqrt{2}\hbar v/l_B$ ,  $l_B = \sqrt{\hbar/eB}$ , and

$$\text{sgn}_\pm(n) = \begin{cases} +1 & (n > 0); \\ \pm 1 & (n = 0); \\ -1 & (n < 0). \end{cases}\tag{8}$$

The Landau levels of  $n \neq 0$  are doubly degenerate between the  $K$  and  $K'$  valleys, while those of  $n = 0$  are not. Figure 1(a) shows an example of energy levels at  $\hbar\omega_B = 2\Delta$ . The thermodynamical potential at temperature  $T$  becomes

$$\Omega = -\frac{1}{\beta} \frac{g_v g_s}{2\pi l_B^2} \sum_{s=\pm} \sum_{n=0}^\infty \varphi[\epsilon_s((\hbar\omega_B)^2 n)] \left(1 - \frac{\delta_{n0}}{2}\right),\tag{9}$$

where  $\beta = 1/k_B T$ ,  $\epsilon_s(x) = s\sqrt{x + \Delta^2}$ ,  $\varphi(\epsilon) = \log[1 + e^{-\beta(\epsilon - \zeta)}]$  with  $\zeta$  being the chemical potential, and  $g_s = 2$  and  $g_v = 2$  represent the degrees of freedom associated with spin and valley, respectively. The magnetic susceptibility is defined by

$$\chi = -\left(\frac{\partial^2 \Omega}{\partial B^2}\right)_\zeta \Big|_{B=0}.\tag{10}$$

In weak magnetic field, using the Euler-Maclaurin formula, the summation in  $n$  in Eq. (9) can be written as an integral in continuous variable  $x$  and a residual term proportional to  $B^2$ . At zero temperature, we have (25)

$$\chi(\epsilon_F) = -g_v g_s \frac{e^2 v^2}{6\pi c^2} \frac{1}{2\Delta} \theta(\Delta - |\epsilon_F|).\tag{11}$$

In the limit of  $\Delta \rightarrow 0$ , this approaches

$$\chi(\epsilon_F) = -g_v g_s \frac{e^2 v^2}{6\pi c^2} \delta(\epsilon_F).\tag{12}$$

The susceptibility of Eq. (11) and the density of states of Eq. (4) are shown in Fig. 1 (b). The susceptibility is not zero in the gap, because the completely filled valence band gives a constant diamagnetic susceptibility. When the Fermi energy enters the conduction band, the susceptibility jumps downs to zero, resulting in zero total magnetism. Because the Hamiltonian is equivalent to that of a Dirac electron with a nonzero mass, the magnetic susceptibility around the band edge should correspond to that of a conventional electron. This is clearly illustrated by the effective Hamiltonian expanded in the vicinity of

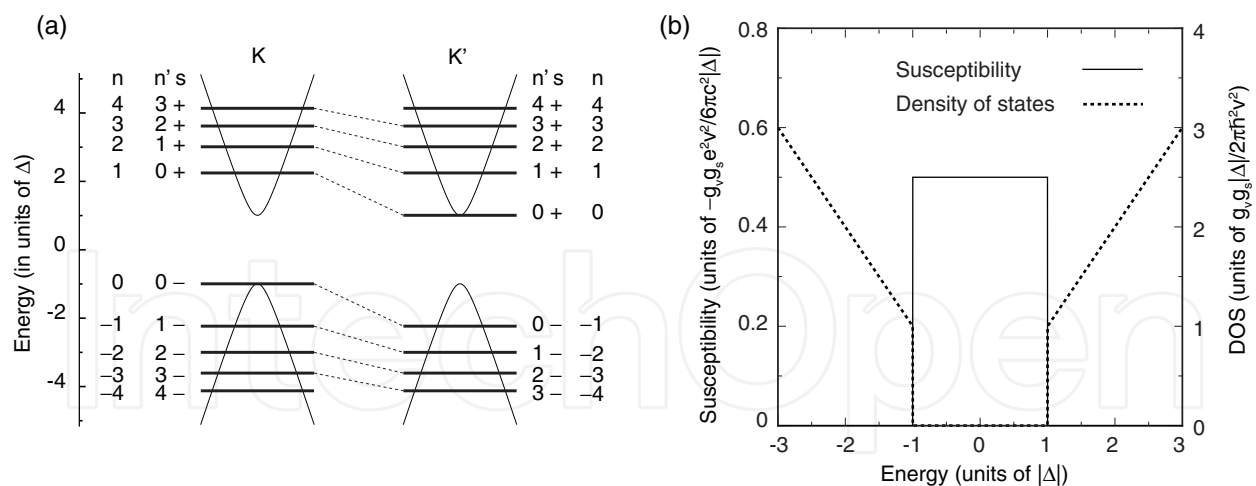


Fig. 1. (a) Landau-level energies of gapped monolayer graphene for  $\hbar\omega_B = 2\Delta$ . (b) Orbital susceptibility (solid) and density of states (dashed) of monolayer graphene with asymmetric potential  $\Delta$ . For susceptibility, the upward direction represents negative (i.e., diamagnetic).

$\mathbf{k} = 0$ . (25) For the conduction band, the effective Hamiltonian for the A site near the band bottom ( $\varepsilon = \Delta$ ) is written apart from the constant energy as

$$\mathcal{H}^K \approx \frac{v^2}{2\Delta} \pi_- \pi_+ = \frac{\pi^2}{2m^*} + \frac{1}{2} g^* \mu_B B, \quad (13)$$

$$\mathcal{H}^{K'} \approx \frac{v^2}{2\Delta} \pi_+ \pi_- = \frac{\pi^2}{2m^*} - \frac{1}{2} g^* \mu_B B, \quad (14)$$

where  $\mu_B = e\hbar/(2mc)$  is the Bohr magneton with  $m$  being the free electron mass, and we defined  $m^* = \Delta/v^2$ ,  $g^* = 2m/m^*$ . For instance, the  $g$  factor is estimated at  $g^* \sim 60$  at  $\Delta = 0.1$  eV, and diverges as  $\propto \Delta^{-1}$  as the gap decreases. The last term in each Hamiltonian can be regarded as the pseudo-spin Zeeman term, where the different valleys  $K$  and  $K'$  serve as pseudo-spin up ( $\zeta = +1$ ) and down ( $\zeta = -1$ ), respectively. This agrees with the Zeeman energy expected for an intrinsic magnetic moment, that originates from the self-rotation of the wave packet in Bloch electron. (44; 45)

Obviously, the pseudo-spin Zeeman term gives the Pauli paramagnetism and the first term containing  $\pi^2$  gives the Landau diamagnetism in the usual form as

$$\chi_P(\varepsilon) = \left(\frac{g^*}{2}\right)^2 \mu_B^2 D(\varepsilon), \quad (15)$$

$$\chi_L(\varepsilon) = -\frac{1}{3} \left(\frac{m}{m^*}\right)^2 \mu_B^2 D(\varepsilon), \quad (16)$$

with density of states  $D(\varepsilon) = g_v g_s m^*/(2\pi\hbar^2) \theta(\varepsilon)$ . The total susceptibility  $\chi_P + \chi_L$  actually agrees with the amount of the jump at the conduction band bottom in  $\chi$  of Eq. (11). Because  $g = 2m/m^*$  in the present case, we have  $\chi_L = -\chi_P/3 \propto 1/m^*$  as in the free electron, giving the paramagnetic susceptibility in total. Therefore the susceptibility exhibits a discrete jump toward the paramagnetic direction when the Fermi energy moves off the Dirac point.

In the original Hamiltonian, the Landau-level energies in Eq. (7) can be rewritten as

$$\varepsilon_{\xi,s,n'} = s \sqrt{(\hbar\omega_B)^2 \left( n' + \frac{1}{2} + \frac{\xi s}{2} \right) + \Delta^2} \quad (n' = 0, 1, 2, \dots). \quad (17)$$

Figure 1(a) shows energy levels for  $\hbar\omega_B = 2\Delta$  and the relationship between the different labeling schemes of Eqs. (7) and (17). For the conduction band, the levels of the same  $n'$  with opposite pseudo-spins  $\xi = \pm 1$  share the same Landau level function labeled by  $n'$  on the  $A$  site, on which the states near the conduction-band bottom ( $\varepsilon = \Delta$ ) have most of the amplitude. For the valence band, similarly,  $n'$  describes the index of the Landau-level function at the  $B$  site.

## 2.2 Response to non-uniform magnetic field

We extend the argument to spatially modulated magnetic fields. The graphene in a non-uniform magnetic field was studied in the context of the electron confinement, (46–48) the peculiar band structures in superlattice, (49; 50) transport, (51) and the quantum Hall effect. (52; 53) In the following, we introduce a linear response theory to general field distributions. (24) We consider an isotropic 2D system, under a magnetic field given by  $B(\mathbf{r}) = [\nabla \times \mathbf{A}(\mathbf{r})]_z$  with vector potential  $\mathbf{A}(\mathbf{r})$ . Here  $\mathbf{r} = (x, y)$  denotes 2D position on the graphene. We define  $\mathbf{j}(\mathbf{r}) = (j_x, j_y)$  as the 2D electric current density induced in the system. Within the linear response, the Fourier-transforms of  $\mathbf{j}(\mathbf{r})$  and  $\mathbf{A}(\mathbf{r})$  satisfy

$$j_\mu(\mathbf{q}) = \sum_\nu K_{\mu\nu}(\mathbf{q}) A_\nu(\mathbf{q}), \quad (18)$$

with response function  $K_{\mu\nu}$ . The gauge invariance for  $\mathbf{A}$  requires  $\sum_\nu K_{\mu\nu}(\mathbf{q}) q_\nu = 0$ , and the continuous equation,  $\nabla \cdot \mathbf{j}(\mathbf{r}) = 0$ , imposes another constraint  $\sum_\mu q_\mu K_{\mu\nu}(\mathbf{q}) = 0$ . To meet both requirements, tensor  $K_{\mu\nu}$  needs to be in the form,

$$K_{\mu\nu}(\mathbf{q}) = K(q) \left( \delta_{\mu\nu} - \frac{q_\mu q_\nu}{q^2} \right). \quad (19)$$

On the other hand, because  $\nabla \cdot \mathbf{j}(\mathbf{r}) = 0$ , we can express  $\mathbf{j}(\mathbf{r})$  as  $j_x = c \partial m / \partial y$ ,  $j_y = -c \partial m / \partial x$ , with  $m(\mathbf{r})$  being the local magnetic moment perpendicular to the layer. In the linear response, its Fourier transform is written as

$$m(\mathbf{q}) = \chi(q) B(\mathbf{q}), \quad (20)$$

with the magnetic susceptibility  $\chi(q)$ . Equations (18) and (20) are complementary, and both response functions  $\chi(q)$  and  $K(q)$  are related by

$$\chi(q) = \frac{1}{cq^2} K(q). \quad (21)$$

We apply the above formulation to graphene without gap, i.e.,  $\Delta = 0$ . The eigenstates at zero magnetic field are labeled by  $(s, \mathbf{k})$  with  $s = +1$  and  $-1$  being the conduction and valence bands, respectively, and wave vector  $\mathbf{k}$ . The eigen energy is given by  $\varepsilon_{s\mathbf{k}} = s\hbar v k$ , and the corresponding wavefunction is  $\psi_{s\mathbf{k}}(\mathbf{r}) = e^{i\mathbf{k} \cdot \mathbf{r}} \mathbf{F}_{s\mathbf{k}} / \sqrt{S}$  with  $\mathbf{F}_{s\mathbf{k}} = \frac{1}{\sqrt{2}} \begin{pmatrix} e^{i\theta} \\ s \end{pmatrix}$ , where  $k$  and  $\theta$  are defined by  $(k_x, k_y) = k(\cos \theta, \sin \theta)$  and  $S$  is the system area.



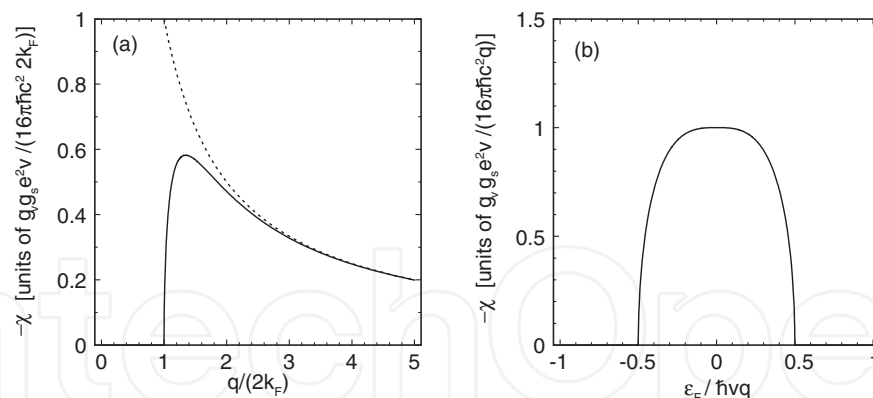


Fig. 2. Magnetic susceptibility  $\chi(q; \varepsilon_F)$  in graphene plotted against (a)  $q$  with fixed  $\varepsilon_F$ , and (b)  $\varepsilon_F$  with fixed  $q$ . Dotted line in (a) represents the undoped case, Eq. (24).

The local current density at  $\mathbf{r}_0$  is calculated as the expectation value of current-density operator  $\hat{\mathbf{j}}(\mathbf{r}_0) = ev \sigma \delta(\mathbf{r} - \mathbf{r}_0)$  over the occupied states. In the first order perturbation in  $\mathbf{A}$ , we have

$$K_{\mu\nu}(\mathbf{q}) = -\frac{g_v g_s e^2}{c} \frac{1}{S} \sum_{ss'\mathbf{k}} \frac{f(\varepsilon_{s\mathbf{k}}) - f(\varepsilon_{s'\mathbf{k}+\mathbf{q}})}{\varepsilon_{s\mathbf{k}} - \varepsilon_{s'\mathbf{k}+\mathbf{q}}} (\mathbf{F}_{s\mathbf{k}}^\dagger v_\nu \mathbf{F}_{s'\mathbf{k}+\mathbf{q}}) (\mathbf{F}_{s'\mathbf{k}+\mathbf{q}}^\dagger v_\mu \mathbf{F}_{s\mathbf{k}}), \quad (22)$$

where  $v_\mu = v\sigma_\mu$ .

At the zero temperature, this can be explicitly calculated as

$$\chi(q; \varepsilon_F) = -\frac{g_v g_s e^2 v}{16\hbar c^2} \frac{1}{q} \theta(q - 2k_F) \left[ 1 + \frac{2}{\pi} \frac{2k_F}{q} \sqrt{1 - \left(\frac{2k_F}{q}\right)^2} - \frac{2}{\pi} \sin^{-1} \frac{2k_F}{q} \right], \quad (23)$$

where  $k_F = |\varepsilon_F|/(\hbar v)$  is the Fermi wave number. Significantly,  $\chi$  vanishes in range  $q < 2k_F$ , i.e., no current is induced when the external field is smooth enough compared to the Fermi wavelength. At  $\varepsilon_F = 0$ , particularly, we have

$$\chi(q; 0) = -\frac{g_v g_s e^2 v}{16\hbar c^2} \frac{1}{q}. \quad (24)$$

We plot  $\chi(q; \varepsilon_F)$  against (a)  $q$  and (b)  $\varepsilon_F$  in Fig. 2. As a function of  $q$ , the susceptibility suddenly starts from zero at  $q = 2k_F$ , and rapidly approaches the universal curve (24). As a function of  $\varepsilon_F$  with fixed  $q$ , it is nonzero only in a finite region satisfying  $|\varepsilon_F| < \hbar v q/2$ , and its integral over  $\varepsilon_F$  becomes constant  $-g_v g_s e^2 v^2/(6\pi c^2)$ . Thus, in the limit of  $q \rightarrow 0$  it goes to the previous result Eq. (12). The susceptibility of the carbon nanotube to a uniform field perpendicular to the axis has the equivalent expression of Eq. (24) where  $q$  is replaced by  $2\pi/L$  with tube circumference  $L$ . (54; 55)

The undoped graphene ( $\varepsilon_F = 0$ ) has a special property in which the counter magnetic field induced by the response current has a spacial distribution similar to that of external magnetic field, regardless of its length scale (24). Let us assume that a sinusoidal external field  $B(\mathbf{r}) = B \cos qx$  is applied to undoped graphene. With the susceptibility Eq. (24), the response current is calculated as  $j_y(\mathbf{r}) = -[g_v g_s e^2 v B/(16\hbar c)] \sin qx$ . The current induces a counter magnetic field which reduces the original field. The  $z$  component of the induced field on graphene becomes

$$B_{\text{ind}}(\mathbf{r}) = -\alpha_g B(\mathbf{r}), \quad \alpha_g = \frac{2\pi g_v g_s e^2 v}{16\hbar c^2} \approx 4 \times 10^{-5}. \quad (25)$$

Because the ratio is independent of  $q$ , Eq. (25) is actually valid for any external field  $B(\mathbf{r})$ , i.e., the magnetic field on the graphene is always reduced by the same factor  $1 - \alpha_g$ . This property holds whenever  $\chi(q)$  is written as  $C/q$  with constant  $C$ .

The argument of the magnetic field screening can be extended in the three dimensional field distribution. Let us suppose a situation when a certain magnetic object is placed above the undoped graphene ( $z > 0$ ), which produces an external magnetic field  $\mathbf{B}(\rho)$  in 3D space  $\rho = (x, y, z)$ . Then, the followings are concluded: (i) On the other side of the graphene ( $z < 0$ ), the induced field becomes  $-\alpha_g \mathbf{B}(\rho)$ , i.e., the external field is screened by the factor  $1 - \alpha_g$ . (ii) On the same side ( $z > 0$ ), the induced field is given by  $\alpha_g R_z[\mathbf{B}(x, y, -z)]$ , where  $R_z$  is the vector inversion with respect to  $z = 0$ . Namely, this is equivalent to a field of the mirror image of the original object reflected with respect to  $z = 0$ , and reduced by  $\alpha_g$ .

Using the property of magnetic mirroring, we can easily estimate the magnetic repulsive force which works between undoped graphene and magnetic objects. If we put on the top of graphene the permanent magnet with surface magnetic flux  $\sigma_m$ , the repulsive force per unit area is given by  $2\pi\alpha_g\sigma_m^2$ , which is a force between a sheet with magnetic monopole density  $\sigma_m$  and its mirror image with  $\alpha_g\sigma_m$ . At  $\sigma_m$  which amounts to the surface flux 1T (e.g., neodymium magnet), (56) this is as large as 0.16 gram weight /cm<sup>2</sup>, which is surprisingly large as a force generated by a thin film only one atom thick.

The  $1/q$  dependence of  $\chi(q)$ , which is responsible for peculiar diamagnetic responses argued above, is a characteristic property common to general  $k$ -linear Hamiltonian. This can be shown using the scaling argument as follows. We consider an isotropic two-dimensional system, in which Hamiltonian  $\mathcal{H}$  contains only terms linear in  $\pi_x$  and  $\pi_y$ . The velocity operator  $v_\mu = \partial\mathcal{H}/\partial\pi_\mu$  is then a constant matrix independent of  $\pi$ . Similarly to graphene, the eigen energy and the wavefunction are written as  $\varepsilon_{n,\mathbf{k}}$  and  $\psi_{n,\mathbf{k}}(\mathbf{r}) = e^{i\mathbf{k}\cdot\mathbf{r}} \mathbf{F}_{n,\mathbf{k}}/\sqrt{S}$ , respectively, with the subband index  $n$  and the wavenumber  $\mathbf{k}$ . The response function  $K_{\mu\nu}(\mathbf{q})$  can then be written in the same form as Eq. (22), with index  $s$  replaced with  $n$ .

If we change the energy and wave number scales by an arbitrary factor  $\alpha$  as

$$\varepsilon = \alpha\tilde{\varepsilon}, \quad k_i = \alpha\tilde{k}_i, \quad (26)$$

then the Hamiltonian becomes formally identical under that transformation, since the coefficients of  $k$ -linear terms in the Hamiltonian remain unchanged. The eigen energy and eigen function obey  $\varepsilon_{n,\tilde{\mathbf{k}}} = \varepsilon_{n,\mathbf{k}}/\alpha$  and  $\mathbf{F}_{n,\tilde{\mathbf{k}}} = \mathbf{F}_{n,\mathbf{k}}$ . Using them, we can show that the response function  $K_{\mu\nu}(\mathbf{q})$  scales at zero temperature and at zero Fermi energy as

$$K_{\mu\nu}\left(\frac{\mathbf{q}}{\alpha}\right) = \frac{K_{\mu\nu}(\mathbf{q})}{\alpha}, \quad (27)$$

which allows us to write as  $K(q) = Cq$  with certain number  $C$ . With Eq. (21), the susceptibility  $\chi$  becomes

$$\chi(q) = \frac{C}{cq}. \quad (28)$$

Similar scaling argument also applies to  $\chi(\varepsilon_F)$  at  $q = 0$ , leading to  $\chi(\varepsilon_F) \propto \delta(\varepsilon_F)$  in any  $k$ -linear Hamiltonian. (26)

### 3. Bilayer graphene

Bilayer graphene is a pair of graphene layers arranged in AB (Bernal) stacking and includes  $A_1$  and  $B_1$  atoms on layer 1 and  $A_2$  and  $B_2$  on layer 2. (33–41) The schematics of the AB stacked



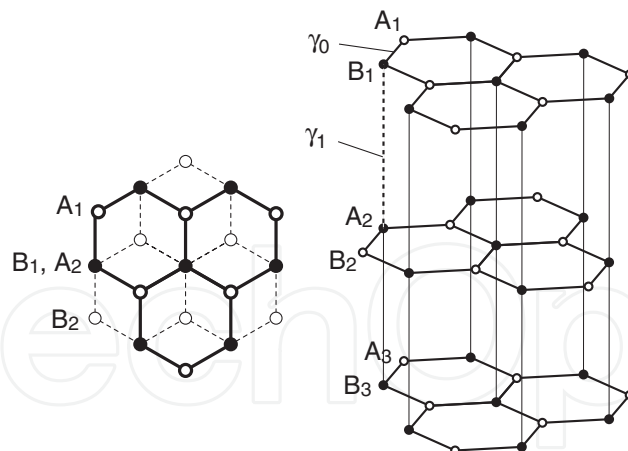


Fig. 3. Atomic structure of AB (Bernal)-stacked multilayer graphene

graphite is illustrated in Figure 3, and the only layer 1 and 2 exist in bilayer graphene. The Hamiltonian at the  $K$  point for the basis  $(|A_1\rangle, |B_1\rangle, |A_2\rangle, |B_2\rangle)$  is given by

$$\mathcal{H}^K = \begin{pmatrix} \Delta & v\pi_- & 0 & 0 \\ v\pi_+ & \Delta & \gamma_1 & 0 \\ 0 & \gamma_1 & -\Delta & v\pi_- \\ 0 & 0 & v\pi_+ & -\Delta \end{pmatrix}, \quad (29)$$

and that for  $K'$  point is obtained by exchanging  $\pi_{\pm}$ . The parameter  $\gamma_1 \approx 0.39$  eV (57) represents vertical coupling between  $B_1$  and  $A_2$  (33; 34; 60), and  $\Delta$  describes potential asymmetry between layer 1 and 2 (not  $A$  and  $B$  sites), which gives rise to an energy gap. (33–37; 39; 60; 61) Experimentally the potential asymmetry can be induced by applying an electric field perpendicular to the layer, (30–32; 62; 63) and the energy gap as large as 0.2 eV was actually observed in spectroscopic measurements. (30; 62; 63) Several interlayer coupling parameters other than  $\gamma_1$  were introduced for the description of the band structure of bulk graphite, (58; 59) while they do not change the qualitative feature of the low-energy spectrum (59) and will be neglected in the following arguments.

The energy band at  $B = 0$  is given by (37)

$$\varepsilon_{s\mu}(p) = s \left( \frac{\gamma_1^2}{2} + v^2 p^2 + \Delta^2 + \mu \left[ \frac{\gamma_1^4}{4} + v^2 p^2 (\gamma_1^2 + 4\Delta^2) \right]^{1/2} \right)^{1/2}, \quad (30)$$

with  $s = \pm 1$  and  $\mu = \pm 1$ . The index  $\mu = +1$  and  $-1$  give a pair of bands further and closer to zero energy, respectively, and  $s = +1$  and  $-1$  in each pair represent the electron and hole branches, respectively. The band-edge energies corresponding to  $p = 0$  are given by  $|\varepsilon| = \varepsilon_{\pm}$  for  $\mu = \pm 1$ , where

$$\varepsilon_+ = \sqrt{\gamma_1^2 + \Delta^2}, \quad \varepsilon_- = |\Delta|. \quad (31)$$

For  $\mu = -1$ , the band minimum becomes

$$\varepsilon_0 = \frac{\gamma_1 |\Delta|}{\sqrt{\gamma_1^2 + 4\Delta^2}}, \quad (32)$$

which corresponds to an off-center momentum. (34) The density of states diverges here as  $D(\varepsilon) \propto (\varepsilon - \varepsilon_0)^{-1/2}$ . The energy bands and the density of states with several  $\Delta$ 's are plotted

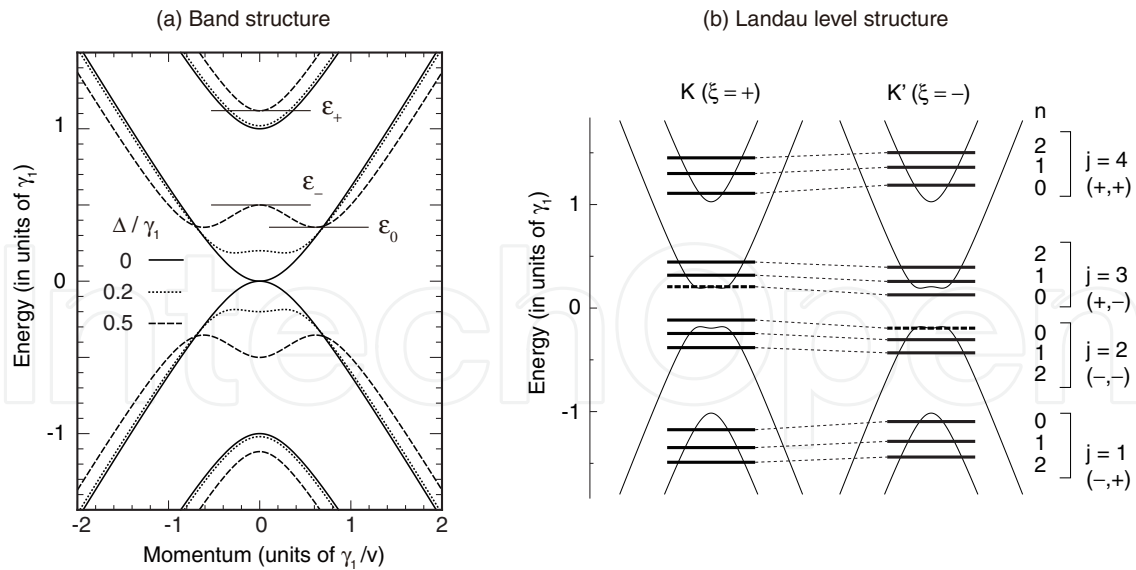


Fig. 4. (a) Band structure of bilayer graphenes with the asymmetry gap  $\Delta/\gamma_1 = 0, 0.2$ , and  $0.5$ . Horizontal lines indicate the energies of  $\epsilon_0, \epsilon_-$  and  $\epsilon_+$  for  $\Delta/\gamma_1 = 0.5$ . (b) Landau-level energies of bilayer graphene given by Eq. (39) with  $\Delta = 0.2\gamma_1$  and  $\hbar\omega_B = 0.5\gamma_1$ . At each valley, an energy level indicated as broken bar represents the Landau level which originally belongs to  $n = -1$  at opposite valley. The quantum number  $(s, \mu)$  is indicated below  $j$ .

in Figs. 5 (a) and (b), respectively. Vertical lines in (a) indicate the energies of  $\epsilon_0, \epsilon_-$ , and  $\epsilon_+$  for  $\Delta = 0.5\gamma_1$ . In a magnetic field, the eigenfunction of the Hamiltonian at the  $K$  point is written as  $(c_1\phi_{n-1}, c_2\phi_n, c_3\phi_n, c_4\phi_{n+1})$  with integer  $n \geq -1$ . For  $n \geq 1$ , the Hamiltonian matrix for  $(c_1, c_2, c_3, c_4)$  becomes(25; 34; 64)

$$H_{n \geq 1}^K = \begin{pmatrix} \Delta & \hbar\omega_B\sqrt{n} & 0 & 0 \\ \hbar\omega_B\sqrt{n} & \Delta & \gamma_1 & 0 \\ 0 & \gamma_1 & -\Delta & \hbar\omega_B\sqrt{n+1} \\ 0 & 0 & \hbar\omega_B\sqrt{n+1} & -\Delta \end{pmatrix}, \tag{33}$$

For  $n = 0$ , the first component does not actually exist because  $\phi_{-1} = 0$ . The matrix for  $(c_2, c_3, c_4)$  becomes

$$H_0^K = \begin{pmatrix} \Delta & \gamma_1 & 0 \\ \gamma_1 & -\Delta & \hbar\omega_B \\ 0 & \hbar\omega_B & -\Delta \end{pmatrix}. \tag{34}$$

For  $n = -1$ , only the component  $c_4$  survives and the Hamiltonian is

$$H_{-1}^K = -\Delta. \tag{35}$$

For the  $K'$  point, the eigenfunction is written as  $(c_1\phi_{n+1}, c_2\phi_n, c_3\phi_n, c_4\phi_{n-1})$ . For  $n \geq 1$ , the Hamiltonian matrix for  $(c_1, c_2, c_3, c_4)$  is

$$H_{n \geq 1}^{K'} = \begin{pmatrix} \Delta & \hbar\omega_B\sqrt{n+1} & 0 & 0 \\ \hbar\omega_B\sqrt{n+1} & \Delta & \gamma_1 & 0 \\ 0 & \gamma_1 & -\Delta & \hbar\omega_B\sqrt{n} \\ 0 & 0 & \hbar\omega_B\sqrt{n} & -\Delta \end{pmatrix}. \tag{36}$$

For  $n = 0$ , the matrix for  $(c_1, c_2, c_3)$  becomes

$$H_0^{K'} = \begin{pmatrix} \Delta & \hbar\omega_B & 0 \\ \hbar\omega_B & \Delta & \gamma_1 \\ 0 & \gamma_1 & -\Delta \end{pmatrix}, \quad (37)$$

and for  $n = -1$ , that for  $c_1$  is

$$H_{-1}^{K'} = \Delta. \quad (38)$$

If we extend the definition of the matrix of Eq. (33) to  $n = 0$ , its three eigenvalues agree with those of  $H_0^K$  and the rest with that of  $H_{-1}^{K'}$ . Similarly, the matrix of Eq. (36) with  $n = 0$  gives eigenvalues of  $H_0^{K'}$  and  $H_{-1}^K$ . Thus we can use Eqs. (33) and (36) with  $n \geq 0$  to produce the full spectrum. By introducing the pseudo-spin variable  $\xi = \pm 1$ , the Hamiltonian is combined into a single expression,

$$H_n^\xi = \begin{pmatrix} \Delta & \sqrt{x_{n-}} & 0 & 0 \\ \sqrt{x_{n-}} & \Delta & \gamma_1 & 0 \\ 0 & \gamma_1 & -\Delta & \sqrt{x_{n+}} \\ 0 & 0 & \sqrt{x_{n+}} & -\Delta \end{pmatrix}, \quad (39)$$

with

$$x_{n\pm} = x_n \pm \frac{1}{2}\xi\delta, \quad (40)$$

and

$$x_n = \left(n + \frac{1}{2}\right)\delta, \quad \delta = (\hbar\omega_B)^2. \quad (41)$$

We write the eigenvalues of  $H_n^\xi$  as

$$\varepsilon_j(x_n, \xi\delta) \quad (j = 1, 2, 3, 4), \quad (42)$$

in the ascending order in energy ( $j = 1$  and  $2$  for valence bands and  $j = 3$  and  $4$  for the conduction bands). The second argument in  $\varepsilon_j(x_n, \xi\delta)$  represents the dependence on  $B$  which are not included in  $x_n$ . Figure 4 shows the example of the Landau-level spectrum at  $\Delta/\gamma_1 = 0.2$  and  $\hbar\omega_B/\gamma_1 = 0.5$ , where the thick dashed lines represent the Landau level which originally belongs to  $n = -1$  at opposite valleys. The correspondence between quantum numbers  $j$  and  $(s, \mu)$  are indicated in the figure.

The thermodynamic potential becomes

$$\begin{aligned} \Omega &= -\frac{1}{\beta} \frac{g_s}{2\pi l_B^2} \sum_{\xi, j} \sum_{n=0}^{\infty} \varphi[\varepsilon_j(x_n, \xi\delta)] \\ &= -\frac{1}{\beta} \frac{g_s}{4\pi\hbar^2 v^2} \sum_{\xi, j} \left[ \int_0^\infty \varphi[\varepsilon_j(x, \xi\delta)] dx + \frac{\delta^2}{24} \frac{\partial \varphi[\varepsilon_j(x, 0)]}{\partial x} \Big|_{x=0} \right] + O(\delta^3), \end{aligned} \quad (43)$$

where we used the Euler-Maclaurin formula in the second equation. The first term in the bracket can be transformed by changing the integral variable from  $x$  to  $\varepsilon$  as

$$\frac{1}{\beta} \int_0^\infty \varphi[\varepsilon_j(x, \xi\delta)] dx = \int_{-\infty}^\infty f(\varepsilon) n_j(\varepsilon, \xi\delta) d\varepsilon, \quad (44)$$

where we used  $\varphi'(\varepsilon) = -\beta f(\varepsilon)$  with  $f(\varepsilon)$  being the Fermi distribution function, and defined

$$n_j(\varepsilon, \zeta\delta) \equiv s_j(\varepsilon, \zeta\delta)x_j(\varepsilon, \zeta\delta), \quad (45)$$

where  $x_j(\varepsilon, \zeta\delta)$  is a real and positive solution of  $\varepsilon = \varepsilon_j(x, \zeta\delta)$  and

$$s_j(\varepsilon, \zeta\delta) \equiv \text{sgn}\left(\frac{\partial x_j(\varepsilon, \zeta\delta)}{\partial \varepsilon}\right). \quad (46)$$

If there are more than one solution of  $x_j$ , we regard  $n_j$  as their sum. The quantity  $n_j(\varepsilon, \zeta\delta)/(4\pi\hbar^2v^2)$  represents the electron density below  $\varepsilon$  for the conduction band and the hole density above  $\varepsilon$  for the valence band. By expanding

$$n_j(\varepsilon, \zeta\delta) = n_j^{(0)}(\varepsilon) + n_j^{(1)}(\varepsilon)\zeta\delta + \frac{1}{2}n_j^{(2)}(\varepsilon)\delta^2 + \dots, \quad (47)$$

we can further expand  $\Omega$  of Eq. (43) in terms of  $\delta \propto B$ . We have (25)

$$\chi(\varepsilon) = g_s g_v \frac{e^2 v^2}{\pi c^2} \sum_j \left[ \int_{-\infty}^{\varepsilon} n_j^{(2)}(\varepsilon') d\varepsilon' - \frac{1}{12} \theta[\varepsilon - \varepsilon_j(0, 0)] \frac{\partial \varepsilon_j(x, 0)}{\partial x} \Big|_{x=0} \right]. \quad (48)$$

For the Hamiltonian of Eq. (39), the eigenequation  $\det(\varepsilon - H_n^{\zeta}) = 0$  can be solved for  $x$  ( $\equiv x_n$ ) as

$$x_{\pm} = \varepsilon^2 + \Delta^2 \pm \frac{1}{2} \sqrt{(4\varepsilon\Delta - \zeta\delta)^2 + 4\gamma_1^2(\varepsilon^2 - \Delta^2)}, \quad (49)$$

which gives  $x_j(\varepsilon, \zeta\delta)$  when being real and positive. At symmetric bilayer,  $\Delta = 0$ , the susceptibility can be explicitly calculated as

$$\chi(\varepsilon) = -\frac{g_v g_s}{4\pi c^2} \frac{e^2 \gamma^2}{\hbar^2} \frac{\theta(\gamma_1 - |\varepsilon_F|)}{\gamma_1} \left( -\ln \frac{|\varepsilon_F|}{\gamma_1} - \frac{1}{3} \right), \quad (50)$$

agreeing with the previous results (15; 21). The susceptibility diverges logarithmically toward  $\varepsilon_F = 0$ , becomes slightly positive for  $|\varepsilon_F| \lesssim \gamma_1$ , and vanishes for  $|\varepsilon_F| > \gamma_1$  where the higher subband enters. The integration of  $\chi$  in Eq. (50) over the Fermi energy becomes  $-(g_v g_s / 3\pi)(e^2 \gamma^2 / \hbar^2)$  independent of  $\gamma_1$ , which is exactly twice as large as that of the monolayer graphene Eq. (12).

For finite asymmetry  $\Delta$ , we can analytically argue several important properties as follows. (25) Let us first consider the case  $\varepsilon > \varepsilon_+$ , where two conduction bands are occupied by electrons. In this case  $x_{\pm}$  are both real and positive and we have  $x_1 = x_2 = 0$ ,  $x_3 = x_+$ , and  $x_4 = x_-$ . Then, we have

$$\sum_j n_j(\varepsilon, \zeta\delta) = x_+ + x_- = 2(\varepsilon^2 + \Delta^2), \quad (51)$$

independent of  $\zeta\delta$ . Therefore,  $\sum_j n_j^{(2)}(\varepsilon)$  identically vanishes, resulting in susceptibility independent of energy in the region  $\varepsilon > \varepsilon_+$  regardless of the value of  $\Delta$ . The same is true for  $\varepsilon < -\varepsilon_+$ . Because  $\chi = 0$  for  $\varepsilon = \pm\infty$ , i.e., in the case of empty or filled band, we can conclude that the susceptibility vanishes for  $\varepsilon > \varepsilon_+$  and  $\varepsilon < -\varepsilon_+$  independent of interlayer interaction  $\gamma_1$  and asymmetry  $\Delta$ .

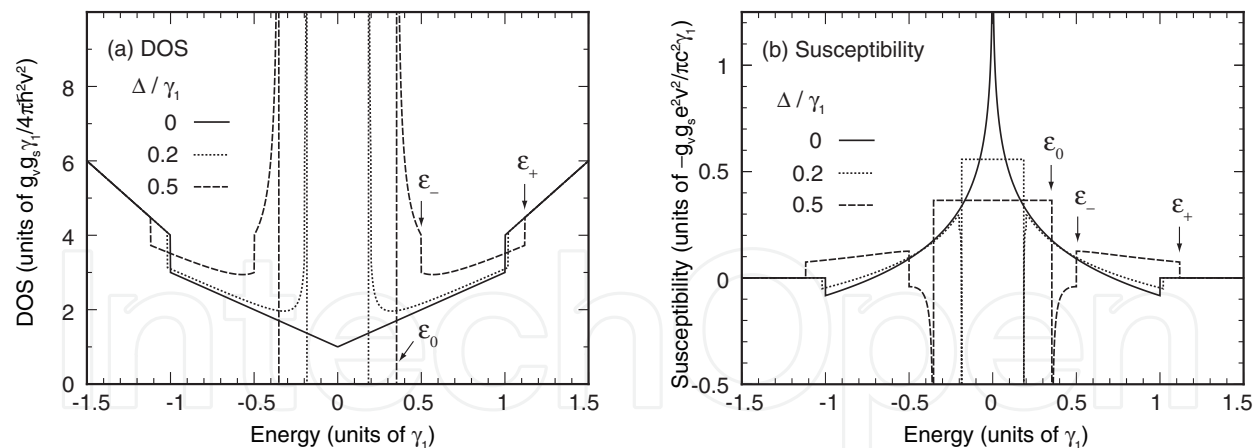


Fig. 5. (a) Density of states, and (b) magnetic susceptibility of bilayer graphenes with the asymmetry gap  $\Delta/\gamma_1 = 0, 0.2$ , and  $0.5$ . Arrows indicate the energies of  $\varepsilon_0$ ,  $\varepsilon_-$  and  $\varepsilon_+$  for  $\Delta/\gamma_1 = 0.5$ . In (b), upward direction represents negative (i.e., diamagnetic) susceptibility.

In the energy region  $-\varepsilon_- < \varepsilon < -\varepsilon_0$  near the top of the valence band, both  $x_+$  and  $x_-$  are real and positive, giving the states at outer and inner equi-energy circle of the band  $j = 2$ , respectively. Then we have

$$n_2^{(2)}(\varepsilon) = \frac{\partial^2}{\partial \delta^2}(-x_+ + x_-) \Big|_{\delta=0} = \frac{\gamma_1^2(\Delta^2 - \varepsilon^2)}{2[(4\Delta^2 + \gamma_1^2)(\varepsilon^2 - \varepsilon_0^2)]^{3/2}}. \quad (52)$$

When the energy approaches to  $-\varepsilon_0$  from the negative side, the integral of  $n_2^{(2)}(\varepsilon)$ , thus the susceptibility, diverges in positive direction as  $\propto (\varepsilon + \varepsilon_0)^{-1/2}$  in the same manner as the density of states. The same divergence occurs at the bottom of the conduction band,  $+\varepsilon_0$ , because of the electron-hole symmetry.

In the vicinity of the bottom of the excited conduction band,  $\varepsilon = \varepsilon_+$ , we have

$$n_4^{(2)}(\varepsilon) = \frac{\partial^2}{\partial \delta^2} x_- \theta(x_-) \Big|_{\delta=0} = \left[ \frac{\partial^2 x_-}{\partial \delta^2} \theta(x_-) + \left( \frac{\partial x_-}{\partial \delta} \right)^2 \delta(x_-) \right]_{\delta=0}, \quad (53)$$

where we used  $x_- \delta(x_-) = 0$  and  $x_- \delta'(x_-) = -\delta(x_-)$ . Using Eq. (48), we find that the susceptibility makes a discrete jump at  $\varepsilon_+$  as

$$\chi(\varepsilon_+ + 0) - \chi(\varepsilon_+ - 0) = g_v g_s \frac{e^2 v^2}{\pi c^2} \left( \frac{\Delta^2 \sqrt{\Delta^2 + \gamma_1^2}}{\gamma_1^2 (2\Delta^2 + \gamma_1^2)} - \frac{2\Delta^2 + \gamma_1^2}{12\gamma_1^2 \sqrt{\Delta^2 + \gamma_1^2}} \right), \quad (54)$$

where the first term in the bracket comes from the integral of the delta function in Eq. (53) and the second term from the step function in Eq. (48).

Near  $\varepsilon_+$ , the eigenstates are given primarily by the dimer states composed of  $|B_1\rangle$  and  $|A_2\rangle$ . The effective Hamiltonian is described by the second order in interband interaction with the conduction-band bottom  $|A_1\rangle$  and the valence-band top  $|B_2\rangle$ , where each process gives a term  $\propto \pi_+ \pi_-$  or  $\propto \pi_- \pi_+$ . In symmetric bilayer with  $\Delta = 0$ , the terms  $\pi_+ \pi_-$  and  $\pi_- \pi_+$  have the same coefficient and the pseudo-spin Zeeman term identically vanishes. When  $\Delta$  becomes nonzero, the two coefficients shift from each other linearly in  $\Delta$  because of the band-gap

opening, leading to a nonzero Zeeman term. The resulting effective Hamiltonian is given by Eqs. (13) and (14) with

$$m^* = \frac{\gamma_1^2 \sqrt{\Delta^2 + \gamma_1^2}}{2v^2(2\Delta^2 + \gamma_1^2)}, \quad g^* = \frac{4\Delta \sqrt{\Delta^2 + \gamma_1^2}}{2\Delta^2 + \gamma_1^2} \frac{m}{m^*}. \quad (55)$$

In the region  $\Delta \lesssim \gamma_1$ , the typical magnitude of the effective mass  $m^*$  is of the order of  $\sim \gamma_1/(2v^2) \approx 0.035m$ .

The susceptibility is written as Pauli and Landau magnetism in Eqs. (15) and (16), respectively, which together give a susceptibility jump of Eq. (54). The paramagnetic component  $\chi_P$  is zero at  $\Delta = 0$  and monotonically increases as  $\Delta$  becomes larger. At  $g^* = (2/\sqrt{3})(m/m^*)$  or  $\Delta \approx 0.34\gamma_1$ ,  $\chi_P$  exceeds  $\chi_L$  and the susceptibility step changes from diamagnetic to paramagnetic. In the limit  $\Delta \rightarrow \infty$ , we have  $g^* = 2m/m^*$  as in the monolayer. This is to be expected, because the bilayer graphene in this limit can be regarded as a pair of independent monolayer graphenes, where interlayer coupling  $\gamma_1$  opens an energy gap at each Dirac point. Similar argument also applies to the behavior around  $\varepsilon_-$ .

Figure 5 (c) plots the susceptibility for  $\Delta = 0, 0.2$ , and  $0.5$ . In accordance with the above analytic consideration, we actually observe that the susceptibility vanishes in the region  $\varepsilon > \varepsilon_+$  and  $\varepsilon < -\varepsilon_+$  and that the susceptibility step at  $\varepsilon = \varepsilon_+$  changes from diamagnetic to paramagnetic with increasing  $\Delta$ . We also see that the susceptibility for  $\Delta \neq 0$  diverges in the paramagnetic direction at  $\varepsilon = \pm\varepsilon_0$ .

#### 4. Multilayer graphenes

We consider a multilayer graphene composed of  $N$  layers of a carbon hexagonal network, which are arranged in the AB (Bernal) stacking. A unit cell contains  $A_j$  and  $B_j$  atoms on the layer  $j = 1, \dots, N$ . If the basis is taken as  $|A_1\rangle, |B_1\rangle; |A_2\rangle, |B_2\rangle; \dots; |A_N\rangle, |B_N\rangle$ , the Hamiltonian for the multilayer graphene around the  $K$  point becomes (26; 34–36; 40; 41)

$$\mathcal{H} = \begin{pmatrix} H_0 & V & & \\ V^\dagger & H_0 & V^\dagger & \\ & V & H_0 & V \\ & & \ddots & \ddots & \ddots \end{pmatrix}, \quad (56)$$

with

$$H_0 = \begin{pmatrix} 0 & v\pi_- \\ v\pi_+ & 0 \end{pmatrix}, \quad V = \begin{pmatrix} 0 & 0 \\ \gamma_1 & 0 \end{pmatrix}, \quad (57)$$

where  $\pi_\pm = \pi_x \pm i\pi_y$  with  $\boldsymbol{\pi} = -i\hbar\nabla + e\mathbf{A}$  and the vector potential  $\mathbf{A}$ . Here we do not consider the interlayer potential asymmetry. The effective Hamiltonian for  $K'$  is obtained by exchanging  $\pi_+$  and  $\pi_-$ .

Let us define functions

$$f_m(j) = \frac{2}{\sqrt{N+1}} \sin\left(\frac{\pi}{2}j\right) \cos\left[\frac{m\pi}{2(N+1)}j\right], \quad (58)$$

$$g_m(j) = \frac{2}{\sqrt{N+1}} \cos\left(\frac{\pi}{2}j\right) \sin\left[\frac{m\pi}{2(N+1)}j\right]. \quad (59)$$



Here  $j = 1, 2, \dots, N$  is the layer index, and  $m$  is the subsystem index which ranges as

$$m = \begin{cases} 1, 3, 5, \dots, N-1, & N = \text{even} \\ 0, 2, 4, \dots, N-1, & N = \text{odd} \end{cases} \quad (60)$$

Obviously  $f_m(j)$  is zero at even  $j$ , while  $g_m(j)$  is zero at odd  $j$ . We construct the basis by assigning  $f_m(j), g_m(j)$  to each cite as

$$\begin{aligned} |\phi_m^{(A,\text{odd})}\rangle &= f_m(1)|A_1\rangle + f_m(3)|A_3\rangle + \dots, \\ |\phi_m^{(B,\text{odd})}\rangle &= f_m(1)|B_1\rangle + f_m(3)|B_3\rangle + \dots, \\ |\phi_m^{(A,\text{even})}\rangle &= g_m(2)|A_2\rangle + g_m(4)|A_4\rangle + \dots, \\ |\phi_m^{(B,\text{even})}\rangle &= g_m(2)|B_2\rangle + g_m(4)|B_4\rangle + \dots. \end{aligned} \quad (61)$$

The superscript such as (A, odd) indicates that the wavefunction has an amplitude only on  $|A_j\rangle$  with odd  $j$ 's.

In the basis of Eq. (61), the Hamiltonian (56) is decomposed into independent blocks labeled by  $m$ . (26) The subspace of  $m = 0$  is special in that  $g_m(j)$  is identically zero, so that only two bases  $\{|\phi_0^{(A,\text{odd})}\rangle, |\phi_0^{(B,\text{odd})}\rangle\}$  survives in Eq. (61). The Hamiltonian matrix projected on this subspace is written as

$$\mathcal{H}_0 = \begin{pmatrix} 0 & v\pi_- \\ v\pi_+ & 0 \end{pmatrix}, \quad (62)$$

which is equivalent to the Hamiltonian of the monolayer graphene. Note that  $m = 0$  only exists when the total layer number  $N$  is odd as shown in Eq. (60). For  $m \neq 0$ , the projected matrix on  $\{|\phi_m^{(A,\text{odd})}\rangle, |\phi_m^{(B,\text{odd})}\rangle, |\phi_m^{(A,\text{even})}\rangle, |\phi_m^{(B,\text{even})}\rangle\}$  becomes

$$\mathcal{H}_m = \begin{pmatrix} 0 & v\pi_- & 0 & 0 \\ v\pi_+ & 0 & \lambda\gamma_1 & 0 \\ 0 & \lambda\gamma_1 & 0 & v\pi_- \\ 0 & 0 & v\pi_+ & 0 \end{pmatrix}, \quad (63)$$

where  $\lambda \equiv \lambda_m$ , is defined by

$$\lambda_m = 2 \cos \kappa_m, \quad \kappa_m = \frac{\pi}{2} - \frac{m\pi}{2(N+1)}. \quad (64)$$

Eq. (63) is equivalent to the Hamiltonian of a bilayer graphene, except that interlayer-coupling parameters  $\gamma_1$  are multiplied by  $\lambda$ . An odd-layered graphene with  $N = 2M + 1$  is composed of one monolayer-type and  $M$  bilayer-type subsystems, while even-layered graphene with  $N = 2M$  is composed of  $M$  bilayers but no monolayer. Figure 6 shows the low-energy band structures in the multilayer graphenes with  $N = 3, 4$ , and 5.

The eigenstate of a finite-layered graphene can be regarded as a part of a standing wave in 3D limit, which is a superposition of opposite traveling waves with  $\pm k_z$ . The quantity  $\kappa (= \kappa_m)$  in our representation corresponds to the 3D wave number via  $\kappa = |k_z|d$ , with  $d$  being the distance between adjacent layers. Thus the monolayer-type subsystem  $\kappa = \pi/2$  is related to  $H$ -point in the 3D Brillouin zone and  $\kappa = 0$  is to  $K$ -point.

Using the decomposition of the Hamiltonian, the magnetization of the  $N$ -layered graphene can be written as a summation over each sub-Hamiltonian. (26) The contribution from

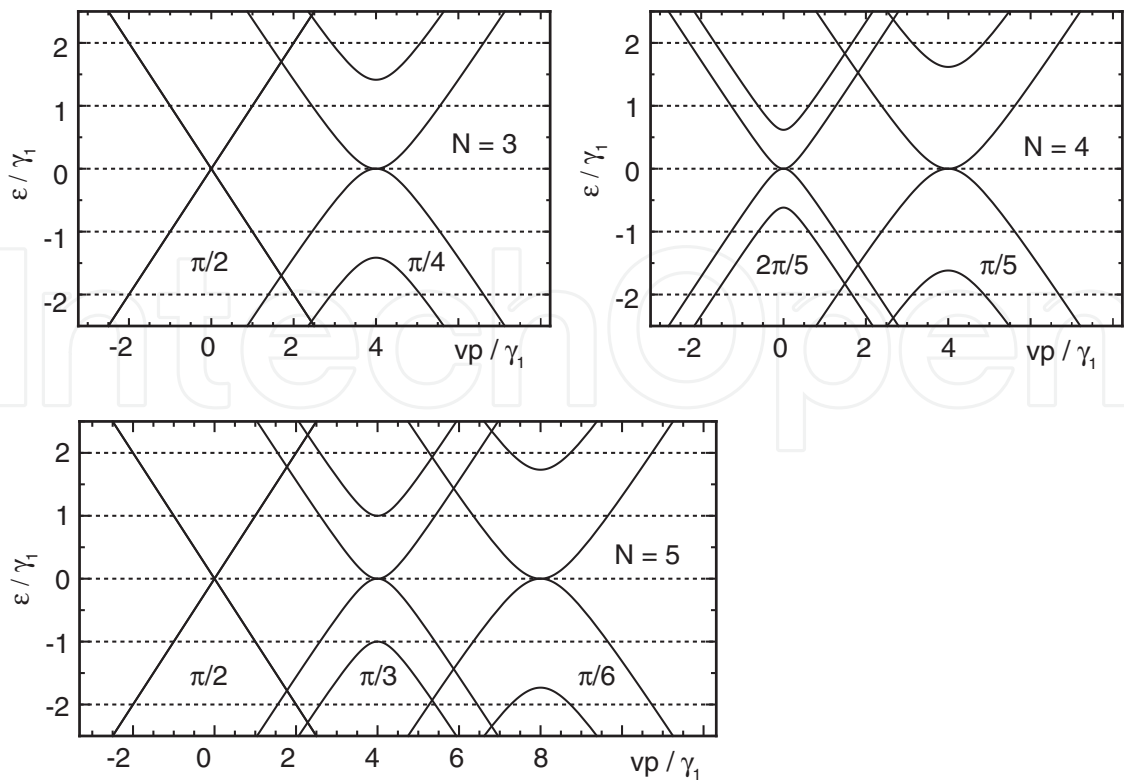


Fig. 6. Band structures of multilayer graphenes of  $N = 3, 4$ , and  $5$ . The energy bands are shown separately for each of subsystems with a horizontal shift. The number represents  $\kappa$ .

$m = 0$  is exactly equivalent to the susceptibility of a monolayer graphene, Eq. (12), which is proportional to delta function of  $\varepsilon_F$ . Thus, the odd-layer graphene always has a large diamagnetic peak at zero energy. The susceptibility of a bilayer-like graphene becomes Eq. (50) with  $\gamma_1$  replaced with  $\lambda\gamma_1$ . Figure 7 shows  $\chi(\varepsilon_F)$  of graphenes with layer number from  $N = 1$  to  $5$ , where we include a constant energy broadening  $\Gamma$  as a phenomenological disorder effect. We can see that odd-layered graphenes exhibit a particularly large peak, which mainly comes from the monolayer-type band.

5. Three dimensional Dirac system

The results of graphene can be directly extended to three-dimensional Dirac Hamiltonian, which approximately describes the electronic structure of bismuth. (4–6; 65) The Hamiltonian is given by

$$\mathcal{H} = \begin{pmatrix} \Delta & 0 & v\pi_z & v\pi_- \\ 0 & \Delta & v\pi_+ & -v\pi_z \\ v\pi_z & v\pi_- & -\Delta & 0 \\ v\pi_+ & -v\pi_z & 0 & -\Delta \end{pmatrix}, \tag{65}$$

where four bases correspond to two orbital and two spin degrees of freedom. The anisotropy of the velocity present in bismuth is ignored for simplicity, as we focus on the parallel argument to its 2D counterpart. The orbital susceptibility was previously calculated for realistic Hamiltonian retaining the anisotropy and other factors. (6)

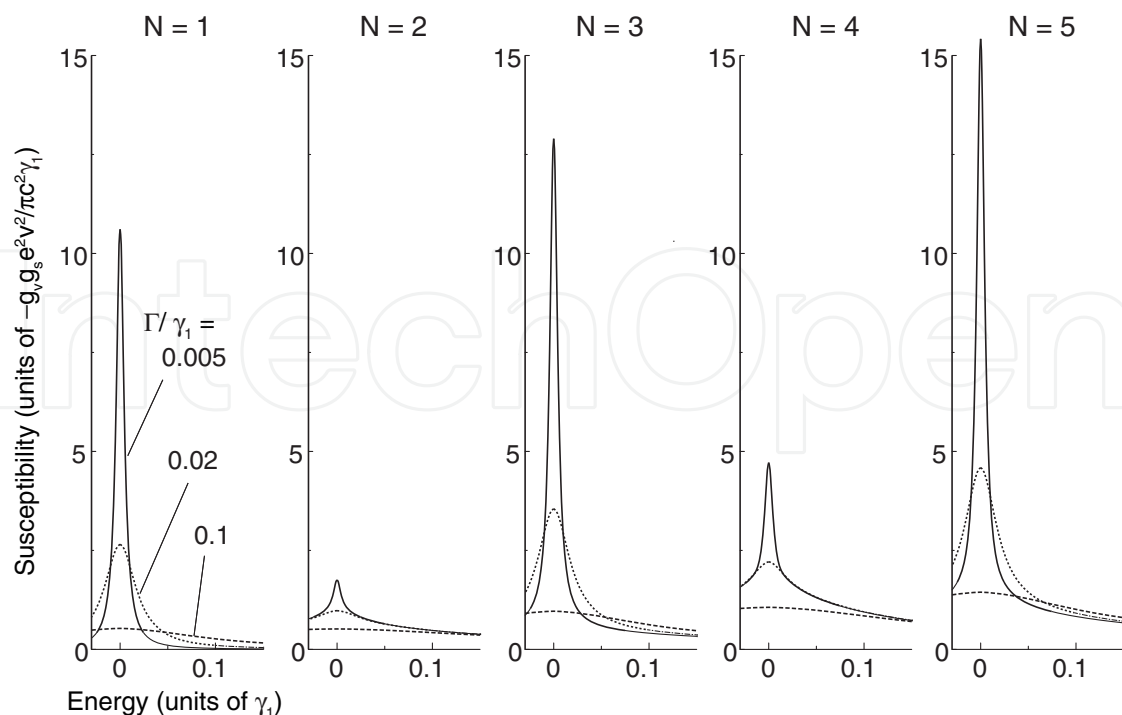


Fig. 7. Susceptibility of multilayer graphenes with layer numbers  $N = 1$  to  $5$ , plotted against the Fermi energy. Results shown for several disorder strengths specified by constant scattering rate  $\Gamma$ .

The density of states at zero magnetic field is

$$D(\varepsilon) = \frac{g_v g_s}{\pi^2 \hbar^3 v^3} |\varepsilon| \sqrt{\varepsilon^2 - \Delta^2} \theta(\varepsilon^2 - \Delta^2), \quad (66)$$

where  $g_v$  is the valley degeneracy allowing the presence of different  $k$  points described by the above Hamiltonian in the first Brillouin zone. The Landau levels in a uniform magnetic field in  $z$  direction are given by (25)

$$\varepsilon_{s,n,\sigma} = s \sqrt{(\hbar\omega_B)^2 \left(n + \frac{1}{2} + \frac{\sigma}{2}\right) + v^2 p_z^2 + \Delta^2} \quad (n = 0, 1, 2, \dots), \quad (67)$$

with  $\hbar\omega_B = \sqrt{2}\hbar v/l_B$ ,  $s = \pm 1$ , and  $\sigma = \pm 1$ . This is equivalent to the two-dimensional Dirac system, Eq. (17), when the term  $\Delta^2$  is replaced with  $\Delta^2 + v^2 p_z^2$ . The susceptibility  $\chi(\varepsilon)$  is calculated by integrating Eq. (11) in  $p_z$  as

$$\begin{aligned} \chi(\varepsilon) &= -\frac{g_v g_s e^2 v^2}{6\pi c^2} \int \frac{dp_z}{2\pi\hbar} \frac{\theta(\Delta^2 + v^2 p_z^2 - \varepsilon^2)}{2\sqrt{\Delta^2 + v^2 p_z^2}} \\ &= -\frac{g_v g_s e^2 v}{12\pi^2 \hbar c^2} \begin{cases} \log \frac{2\varepsilon_c}{|\Delta|} & (|\varepsilon| < |\Delta|); \\ \log \frac{2\varepsilon_c}{|\varepsilon| + \sqrt{\varepsilon^2 - \Delta^2}} & (|\varepsilon| > |\Delta|), \end{cases} \end{aligned} \quad (68)$$

where  $\varepsilon_c$  is a cut-off energy. In the limit of  $\Delta \rightarrow 0$ , the susceptibility at zero energy logarithmically diverges.

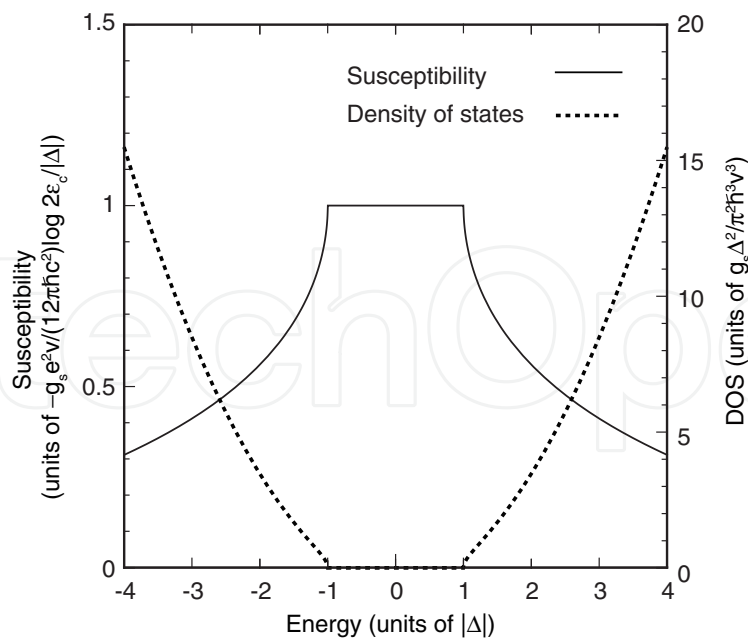


Fig. 8. Orbital susceptibility and density of states of three-dimensional Dirac electron.

At an energy  $\varepsilon$  just above the band bottom  $|\Delta|$ , we obtain the paramagnetic contribution

$$\chi(\varepsilon) - \chi(0) \approx \frac{2}{3} \left( \frac{m}{m^*} \right)^2 D(\varepsilon) \mu_B^2, \tag{69}$$

where  $D(\varepsilon) = (g_s g_v / 4 \pi^2) (2 m^* / \hbar^2)^{3/2} \sqrt{\varepsilon}$  with  $m^* = \Delta / v^2$ . This is nothing but the magnetic susceptibility, dominated by the Pauli paramagnetism, of a three-dimensional metal with mass  $m^*$  and  $g$  factor  $g^* = 2 m / m^*$ . Figure 8 shows the susceptibility and the density of states in the present system. The singular decrease of the susceptibility at the band edges is understood in terms of the appearance of the dominant spin paramagnetism inside the band.

We note that in bismuth the index  $\sigma$  in Eq. (67) represents real spin, while it was valley pseudo-spin in Eq. (17) for graphene. The Pauli component included in Eq. (69) thus describes the real spin paramagnetism enhanced by the strong spin-orbit coupling, apart from the bare electron paramagnetism.

6. Conclusion

We have reviewed the orbital magnetism of graphene and related materials. Graphene monolayer has a delta-function singularity at Dirac point, which can be understood in zero-mass limit of massive Dirac electrons. There the Pauli paramagnetism associated with valley degree of freedom gives an essential contribution in addition to the conventional Landau diamagnetism. The graphene multilayers also exhibits strong diamagnetism, while the interlayer coupling significantly modifies the magnetic singularity at the band touching point. The argument can be extended for a three-dimensional Dirac system, which explains the strong diamagnetism of bismuth in a parallel fashion to that for graphene. The susceptibility in graphene related systems is expected to be observed by employing the experimental techniques used for two-dimensional electron systems in semiconductor.(66–71)

## 7. Acknowledgments

The materials presented here are based on close collaborations with Tsuneya Ando, Yasunori Arimura and Edward McCann. This work was supported in part by Grant-in-Aid for Scientific Research on Priority Area “Carbon Nanotube Nanoelectronics,” by Grant-in-Aid for Scientific Research, by Global Center of Excellence Program at Tokyo Tech “Nanoscience and Quantum Physics” from Ministry of Education, Culture, Sports, Science and Technology Japan, and by EPSRC First Grant EP/E063519/1 and by JST-EPSRC Japan-UK Cooperative Programme Grant EP/H025804/1.

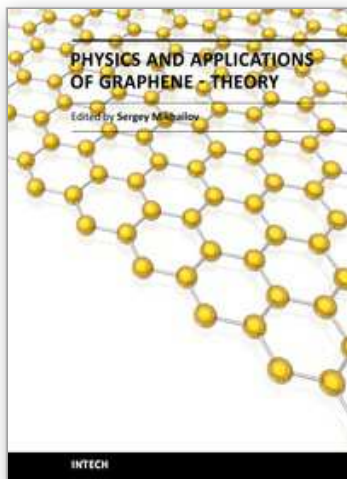
## 8. References

- [1] J. W. McClure, Phys. Rev. 104, 666 (1956).
- [2] J. W. McClure, Phys. Rev. 119, 606 (1960).
- [3] M. P. Sharma, L. G. Johnson, and J. W. McClure, Phys. Rev. B 9, 2467 (1974).
- [4] P. A. Wolff, J. Phys. Chem. Solids 25, 1057 (1964).
- [5] H. Fukuyama and R. Kubo, J. Phys. Soc. Jpn. 27, 604 (1969).
- [6] H. Fukuyama and R. Kubo, J. Phys. Soc. Jpn. 28, 570 (1970).
- [7] K. S. Novoselov, A. K. Geim, S. V. Morozov, D. Jiang, Y. Zhang, S. V. Dubonos, I. V. Grigorieva, and A. A. Firsov, Science 306, 666 (2004).
- [8] K. S. Novoselov, A. K. Geim, S. V. Morozov, D. Jiang, M. I. Katsnelson, I. V. Grigorieva, S. V. Dubonos, and A. A. Firsov, Nature 438, 197 (2005).
- [9] Y. Zhang, Y.-W. Tan, H. L. Stormer, and P. Kim, Nature 438, 201 (2005).
- [10] J. C. Slonczewski and P. R. Weiss, Phys. Rev. 109, 272 (1958).
- [11] D. P. DiVincenzo and E. J. Mele, Phys. Rev. B 29, 1685 (1984).
- [12] G. W. Semenoff, Phys. Rev. Lett. 53, 2449 (1984).
- [13] T. Ando, J. Phys. Soc. Jpn. 74, 777 (2005). Theory of electronic states and transport in carbon nanotubes
- [14] S. A. Safran and F. J. DiSalvo, Phys. Rev. B 20, 4889 (1979).
- [15] S. A. Safran, Phys. Rev. B 30, 421 (1984).
- [16] J. Blinowski and C. Rigaux, J. Phys. (Paris) 45, 545 (1984).
- [17] R. Saito and H. Kamimura, Phys. Rev. B 33, 7218 (1986).
- [18] S. G. Sharapov, V. P. Gusynin, and H. Beck, Phys. Rev. B 69, 075104 (2004). Magnetic oscillations in planar systems with the Dirac-like spectrum of quasiparticle excitations
- [19] H. Fukuyama, J. Phys. Soc. Jpn. 76, 043711 (2007).
- [20] M. Nakamura, Phys. Rev. B 76, 113301 (2007).
- [21] M. Koshino and T. Ando, Phys. Rev. B 75, 235333 (2007).
- [22] A. Ghosal, P. Goswami, and S. Chakravarty, Phys. Rev. B 75, 115123 (2007).
- [23] A. Kobayashi, Y. Suzumura, and H. Fukuyama, J. Phys. Soc. Jpn. 77, 064718 (2008).
- [24] M. Koshino, Y. Arimura, and T. Ando, Phys. Rev. Lett. 102, 177203 (2009).
- [25] M. Koshino and T. Ando, Phys. Rev. B 81, 195431 (2010).
- [26] M. Koshino and T. Ando, Phys. Rev. B 76, 085425 (2007).
- [27] M. Nakamura and L. Hirasawa, Phys. Rev. B 77, 045429 (2008).

- [28] A. H. Castro Neto, F. Guinea, N. M. Peres, K. S. Novoselov, and A. K. Geim, *Rev. Mod. Phys.* 81, 109 (2009).
- [29] K. S. Novoselov, E. McCann, S. V. Morozov, V. I. Falko, M. I. Katsnelson, U. Zeitler, D. Jiang, F. Schedin, and A. K. Geim, *Nature Phys.* 2, 177 (2006).
- [30] T. Ohta, A. Bostwick, T. Seyller, K. Horn, and E. Rotenberg, *Science* 313, 951 (2006)
- [31] E. V. Castro, K. S. Novoselov, S. V. Morozov, N. M. R. Peres, J. M. B. Lopes dos Santos, J. Nilsson, F. Guinea, A. K. Geim, and A. H. Castro Neto, *Phys. Rev. Lett.* 99, 216802 (2007).
- [32] J. B. Oostinga, H. B. Heersche, X.-L. Liu, A. F. Morpurgo, and L. M. K. Vandersypen, *Nat. Mat.* 7, 151 (2008).
- [33] E. McCann and V. I. Falko, *Phys. Rev. Lett.* 96, 086805 (2006).
- [34] F. Guinea, A. H. Castro Neto, and N. M. R. Peres, *Phys. Rev. B* 73, 245426 (2006).
- [35] C. L. Lu, C. P. Chang, Y. C. Huang, J. M. Lu, C. C. Hwang, and M. F. Lin, *J. Phys.: Cond. Matt.* 18, 5849 (2006).
- [36] C. L. Lu, C. P. Chang, Y. C. Huang, R. B. Chen, and M. L. Lin, *Phys. Rev. B* 73, 144427 (2006).
- [37] E. McCann, *Phys. Rev. B* 74, 161403 (2006).
- [38] M. Koshino and T. Ando, *Phys. Rev. B* 73, 245403 (2006).
- [39] J. Nilsson, A. H. Castro Neto, N. M. R. Peres, and F. Guinea, *Phys. Rev. B* 73, 214418 (2006).
- [40] B. Partoens and F. M. Peeters, *Phys. Rev. B* 74, 075404 (2006).
- [41] B. Partoens and F. M. Peeters, *Phys. Rev. B* 75, 193402 (2007).
- [42] S. Y. Zhou, G.-H. Gweon, A. V. Fedorov, P. N. First, W. A. de Heer, D.-H. Lee, F. Guinea, A. H. Castro Neto, and A. Lanzara, *Nature Mater.* 6, 770 (2007).
- [43] S. Y. Zhou, D. A. Siegel, A. V. Fedorov, F. El Gabaly, A. K. Schmid, A. H. Castro Neto, D.-H. Lee, and A. Lanzara, *Nature Mater.* 7, 259 (2008).
- [44] M.-C. Chang and Q. Niu, *Phys. Rev. B* 53, 7010 (1996).
- [45] D. Xiao, W. Yao, and Q. Niu, *Phys. Rev. Lett.* 99, 236809 (2007).
- [46] N. M. R. Peres, F. Guinea, and A. H. Castro Neto, *Phys. Rev. B* 73, 125411 (2006).
- [47] A. De Martino, L. Dell'Anna, and R. Egger, *Phys. Rev. Lett.* 98, 066802 (2007).
- [48] M. R. Masir, P. Vasilopoulos, A. Matulis, and F. M. Peeters, *Phys. Rev. B* 77, 235443 (2008).
- [49] C.-H. Park, L. Yang, Y.-W. Son, M. L. Cohen, and S. G. Louie, *Phys. Rev. Lett.* 101, 126804 (2008).
- [50] C.-H. Park, Y.-W. Son, L. Yang, M. L. Cohen, and S. G. Louie, *Nano Lett.* 8, 2920 (2008).
- [51] Y.-X. Li, *J. Phys.: Condens. Matter* 22, 015302 (2010).
- [52] J. S. Park, K. Sasaki, R. Saito, W. Izumida, M. Kalbac, H. Farhat, G. Dresselhaus, and M. S. Dresselhaus, *Phys. Rev. B* 80, 081402 (2009).
- [53] I. Snymán, *Phys. Rev. B* 80, 054303 (2009).
- [54] H. Ajiki and T. Ando, *J. Phys. Soc. Jpn.* 62, 2470 (1993); *ibid.* 63, 4267 (1994); *ibid.* 64, 4382 (1995).
- [55] M. Yamamoto, M. Koshino, and T. Ando *J. Phys. Soc. Jpn.* 77, 084705 (2008).
- [56] See, for example, J.M.D. Coey: *Rare-earth Iron Permanent Magnets*, (Clarendon Press, 1996)



- [57] A. Misu, E. Mendez, and M. S. Dresselhaus, *J. Phys. Soc. Jpn.* 47, 199 (1979).
- [58] M. S. Dresselhaus and G. Dresselhaus, *Adv. Phys.* 51, 1 (2002).
- [59] M. Koshino and T. Ando, *Solid State Commun.* 149, 1123 (2009).
- [60] T. Ando and M. Koshino, *J. Phys. Soc. Jpn.* 78, 034709 (2009).
- [61] T. Ando and M. Koshino, *J. Phys. Soc. Jpn.* 78, 104716 (2009).
- [62] Y. Zhang, T.-T. Tang, C. Girit, Z. Hao, M. C. Martin, A. Zettl, M. F. Crommie, Y. R. Shen, and F. Wang, *Nature* 459, 820 (2009).
- [63] K. F. Mak, C. H. Lui, J. Shan, and T. F. Heinz, *Phys. Rev. Lett.* 102, 256405 (2009).
- [64] M. Koshino and E. McCann, *Phys. Rev. B* 81, 115315 (2010).
- [65] Y. Fuseya, M. Ogata, and H. Fukuyama, *Phys. Rev. Lett.* 102, 066601 (2009).
- [66] H. L. Stormer, T. Haavasoja, V. Narayanamurti, A. C. Gossard, and W. Wiegmann, *J. Vac. Sci. Technol. B* 1, 423 (1983).
- [67] J. P. Eisenstein, H. L. Stormer, V. Narayanamurti, A. Y. Cho, A. C. Gossard, and C. W. Tu, *Phys. Rev. Lett.* 55, 875 (1985).
- [68] I. Meinel, D. Grundler, S. Bargstadt-Franke, C. Heyn, and D. Heitmann, *Appl. Phys. Lett.* 70, 3305 (1997).
- [69] A. Potts, R. Shepherd, W. G. Herrenden-Harker, M. Elliott, C. L. Jones, A. Usher, G. A. C. Jones, D. A. Ritchie, E. H. Linfield, and M. Grimshaw, *J. Phys. C* 8, 5189 (1996).
- [70] S. A. J. Wieggers, M. Specht, L. P. Levy, M. Y. Simmons, D. A. Ritchie, A. Cavanna, B. Etienne, G. Martinez, and P. Wyder, *Phys. Rev. Lett.* 79, 3238 (1997).
- [71] M. Zhu, A. Usher, A. J. Matthews, A. Potts, M. Elliott, W. G. Herrenden-Harker, D. A. Ritchie, and M. Y. Simmons, *Phys. Rev. B* 67, 155329 (2003).



## **Physics and Applications of Graphene - Theory**

Edited by Dr. Sergey Mikhailov

ISBN 978-953-307-152-7

Hard cover, 534 pages

**Publisher** InTech

**Published online** 22, March, 2011

**Published in print edition** March, 2011

The Stone Age, the Bronze Age, the Iron Age... Every global epoch in the history of the mankind is characterized by materials used in it. In 2004 a new era in material science was opened: the era of graphene or, more generally, of two-dimensional materials. Graphene is the strongest and the most stretchable known material, it has the record thermal conductivity and the very high mobility of charge carriers. It demonstrates many interesting fundamental physical effects and promises a lot of applications, among which are conductive ink, terahertz transistors, ultrafast photodetectors and bendable touch screens. In 2010 Andre Geim and Konstantin Novoselov were awarded the Nobel Prize in Physics "for groundbreaking experiments regarding the two-dimensional material graphene". The two volumes *Physics and Applications of Graphene - Experiments* and *Physics and Applications of Graphene - Theory* contain a collection of research articles reporting on different aspects of experimental and theoretical studies of this new material.

### **How to reference**

In order to correctly reference this scholarly work, feel free to copy and paste the following:

Mikito Koshino (2011). Orbital Magnetism of Graphenes, *Physics and Applications of Graphene - Theory*, Dr. Sergey Mikhailov (Ed.), ISBN: 978-953-307-152-7, InTech, Available from:  
<http://www.intechopen.com/books/physics-and-applications-of-graphene-theory/orbital-magnetism-of-graphenes>

**INTECH**  
open science | open minds

### **InTech Europe**

University Campus STeP Ri  
Slavka Krautzeka 83/A  
51000 Rijeka, Croatia  
Phone: +385 (51) 770 447  
Fax: +385 (51) 686 166  
[www.intechopen.com](http://www.intechopen.com)

### **InTech China**

Unit 405, Office Block, Hotel Equatorial Shanghai  
No.65, Yan An Road (West), Shanghai, 200040, China  
中国上海市延安西路65号上海国际贵都大饭店办公楼405单元  
Phone: +86-21-62489820  
Fax: +86-21-62489821

© 2011 The Author(s). Licensee IntechOpen. This chapter is distributed under the terms of the [Creative Commons Attribution-NonCommercial-ShareAlike-3.0 License](https://creativecommons.org/licenses/by-nc-sa/3.0/), which permits use, distribution and reproduction for non-commercial purposes, provided the original is properly cited and derivative works building on this content are distributed under the same license.

IntechOpen

IntechOpen